Vision Research xxx (xxxx) xxx

Contents lists available at ScienceDirect

Vision Research

journal homepage: www.elsevier.com/locate/visres

Neural processing of bottom-up perception of biological motion under attentional load

Hilal Nizamoglu [a,b,*], Burcu A. Urgen [a,c,d,*]

[a] Interdisciplinary Neuroscience Program, Bilkent University, Ankara, Turkey
[b] Department of Psychology, Justus Liebig University in Giessen, Giessen, Germany
[c] Department of Psychology, Bilkent University, Ankara, Turkey
[d] Aysel Sabuncu Brain Research Center and National Magnetic Resonance Imaging Center, Bilkent University, Ankara, Turkey

ARTICLE INFO

Keywords:
Biological motion
Attentional load
fMRI
MVPA

ABSTRACT

Considering its importance for one's survival and social significance, biological motion (BM) perception is assumed to occur automatically. Previous behavioral results showed that task-irrelevant BM in the periphery interfered with task performance at the fovea. Under selective attention, BM perception is supported by a network of regions including the occipito-temporal (OTC), parietal, and premotor cortices. Retinotopy studies that use BM stimulus showed distinct maps for its processing under and away from selective attention. Based on these findings, we investigated how bottom-up perception of BM would be processed in the human brain under attentional load when it was shown away from the focus of attention as a task-irrelevant stimulus. Participants (N = 31) underwent an fMRI study in which they performed an attentionally demanding visual detection task at the fovea while intact or scrambled point light displays of BM were shown at the periphery. Our results showed the main effect of attentional load in fronto-parietal regions and both univariate activity maps and multivariate pattern analysis results support the attentional load modulation on the task-irrelevant peripheral stimuli. However, this effect was not specific to intact BM stimuli and was generalized to motion stimuli as evidenced by the motion-sensitive OTC involvement during the presence of dynamic stimuli in the periphery. These results confirm and extend previous work by showing that task-irrelevant distractors can be processed by stimulus-specific regions when there are enough attentional resources available. We discussed the implications of these results for future studies.

1. Introduction

Humans and non-human animals are considered to have an innate tendency to detect and discriminate the movements of other living things from the movements of non-living things (such as objects) starting from the early ages of life (Bertenthal, Proffitt, & Kramer, 1987; Fox & McDaniel, 1982; Pavlova, Krägeloh-Mann, Sokolov, & Birbaumer, 2001; Sifre et al., 2018; Simion, Regolin, & Bulf, 2008; Vallortigara, Regolin, & Marconato, 2005). Besides its obvious importance for survival, this skill, also known as the ability to perceive biological motion (BM), constitutes the basis for higher order social skills such as communication and social interaction in humans (Blake & Shiffrar, 2007). One can infer the emotional state (Halovic & Kroos, 2018), gender (Pollick, Kay, Heim, & Stringer, 2005), and age of the person (see Blake & Shiffrar, 2007) as well as their social characteristics such as identity (Yovel & O'Toole, 2016) and personal traits (Thoresen, Vuong, & Atkinson, 2012) even from a simplistic and artificial display of a very basic locomotion action: Point-light displays (PLDs) of walking BM. Because of this ability, even when the observed action is not social in its nature (e.g. waving goodbye), a simple walking BM figure is considered social in the person perception literature (Rutherford & Kuhlmeier, 2013).

According to Thompson and Parasuraman (2012), BM perception requires three main steps of processing: (i) detecting the body features constituting a movement; (ii) forming action representations; and (iii) understanding the intentions conveyed from observed actions. These steps are supported by a network of regions including occipito-temporal cortex (OTC) regions that involve form and motion sensitive areas, including extrastriate body area (EBA) and human middle temporal cortex cluster (hMT+) (Downing, Jiang, Shuman, & Kanwisher, 2001;

* Corresponding authors at: Interdisciplinary Neuroscience Program, Bilkent University, Ankara, Turkey.
E-mail addresses: Hilal.Nizamoglu@psychol.uni-giessen.de (H. Nizamoglu), burcu.urgen@bilkent.edu.tr (B.A. Urgen).

https://doi.org/10.1016/j.visres.2023.108328
Received 11 May 2023; Received in revised form 13 October 2023; Accepted 16 October 2023

Grezes et al., 2001; Grossman & Blake, 2002; Jastorff & Orban, 2009; Peelen, Wiggett, & Downing, 2006; Peuskens, Vanrie, Verfaillie, & Orban, 2005; Pyles & Grossman, 2013; Vangeneugden, Peelen, Tadin, & Battelli, 2014), in addition to superior temporal sulcus (STS) as the integrative hub of encoding these visual features (Felleman & Van Essen, 1991; Jastorff, Popivanov, Vogels, Vanduffel, & Orban, 2012; Oram & Perrett, 1996; Shiffrar, 1994; Vangeneugden et al., 2011; Vangeneugden, Pollick, & Vogels, 2008) to eventually create action representations (Pitcher & Ungerleider, 2021); and finally parietal and frontal regions such as inferior parietal lobule (IPL), anterior intraparietal sulcus (aIPS), inferior frontal gyrus (IFG) and premotor cortex (PMC) that are important for processing higher aspects of observed actions leading to action understanding (Saygin, 2013; Rizzolatti, Fadiga, Gallese, & Fogassi, 1996; Rizzolatti & Craighero, 2004; Urgen & Orban, 2021; de C. Hamilton & Grafton, 2007; Jastorff, Begliomini, Fabbri-Destro, Rizzolatti, & Orban, 2010; Buccino et al., 2001; Wheaton, Thompson, Syngeniotis, Abbott, & Puce, 2004).

This network of regions is consistently evident in the literature that studied the BM stimuli under selective attention (Beauchamp, Lee, Haxby, & Martin, 2003; Grossman & Blake, 2002; Herrington, Nymberg, Faja, Price, & Schultz, 2012; Jastorff & Orban, 2009; Peelen et al., 2006; Saygin, Wilson, Hagler, Bates, & Sereno, 2004; Thornton, 2013; Vaina, Solomon, Chowdhury, Sinha, & Belliveau, 2001). By definition, selective attention is our ability to focus on the task at hand while filtering out the task-irrelevant stimuli. Accordingly, BM perception under selective attention is studied with *active tasks* on BM stimuli such as discrimination based on walking direction, detection of BM under changing contrast, noise mask, or when the motion or form features are disrupted (e.g. inverted stimulus) or have become ambiguous (e.g. opposite motion of local versus global motion of BM stimulus) (Thornton, 2013). In such studies, the focus of attention is right at the BM stimulus itself such that top-down resources are available for BM perception (e.g. in the case of ambiguous stimuli). However, considering the innate tendency of humans to process biological motion, BM perception can occur automatically in an effortless manner (Johansson, 1973; Thompson & Parasuraman, 2012; Thornton, Rensink, & Shiffrar, 2002) even when the attention is directed away from it. Indeed, a behavioral experiment conducted by Thornton and Vuong (2004) showed that when presented as a task-irrelevant distractor at the periphery, BM impaired the performance on a task at the fovea. This finding shows that the "to-be-ignored" peripheral BM stimuli were processed incidentally. The fMRI studies in the literature shows that in such bottom up processing, regions that are activated in response to BM are constrained to OTC regions of the BM perception network. On the other hand, when the selective attention is directed towards the BM stimuli as in the case of active viewing tasks, further regions in addition to the OTC such as fronto-parietal areas were found to be responding that indicates the contribution of higher level processing. More specifically, during passive viewing tasks, the activity maps include the visual feature encoding areas (i.e. EBA, hMT+, FBA) up until STS rather than the aforementioned BM processing areas that reach until fronto-parietal regions. For instance, in the study conducted by Jastorff and Orban (2009), only the occipital and ventral temporal areas (i.e. EBA, hMT+) showed significant activation when participants did not engage in an active task but just passively viewed the BM stimuli. Furthermore, Herrington et al. (2012) compared passive color detection versus active goal understanding task on BM stimuli. They found that right anterior STS, as well as hMT+and EBA activations were stronger in goal understanding compared to the color detection task. Finally, in a retinotopic mapping study, Saygin and Sereno (2008) showed that the spatial extent of retinotopic maps differed depending on whether the participants were engaged in an active task (attention to BM stimuli) or passive task (ignore BM stimuli). When attention is directed towards the BM stimuli on the wedge that swaps the visual field, retinotopic maps were observed in OTC including STS; parietal cortex including IPS and PPC; and frontal cortex including superior precentral sulcus (i.e. frontal eye field [FEF]). However, during the passive viewing task when attention is directed away from the BM stimuli, the retinotopic maps found in all these regions were either reduced or diminished to only OTC regions (V3, hMT+, LOC, STS) and IPS.

Considering the incidental processing of BM and the difference between its underlying neural correlates of top-down and bottom-up perception, one may hypothesize whether more "high-level" regions are affected by selective attention; whereas, feature encoding regions are involved in a rather "automatic" processing. Following this research question, in this study, we examined whether a stimulus that is socially and ecologically important like BM would be processed within the BM perception network when it was shown away from the focus of attention via an attentional load paradigm (Lavie, 1995).

In attentional load paradigms, an irrelevant stimulus is presented at the periphery, while participants are engaged in a visual detection task that demands either high or low attention at the fovea. Load theory proposed by Lavie (1995, 2005) suggests that considering there is a limit to perceptual capacity, the processing of each element within the field of view cannot be processed in the same manner. Attention, in that sense, works as a regulatory mechanism based on task demands (Bruckmaier, Tachtsidis, Phan, & Lavie, 2020). Accordingly, the activation related to the unattended, task-irrelevant stimuli is stronger under low attentional load since there are available attentional resources that can be allocated to these stimuli, while it is decreased or diminished under high load since attentional resources are limited. In the literature, flickering checkerboards, optic flow of lines, and colorful patches have been used as task-irrelevant stimuli on the periphery. The processing of these stimuli were found to be modulated by attentional load at early visual cortex areas (V1–V4), motion sensitive middle temporal (MT) cortex, and color responsive area V4, respectively (see Schwartz et al., 2004; Rees, Frith, & Lavie, 1997; Desseilles et al., 2009). By examining whether BM will be processed at the periphery through an attentional load experiment, this study is first to show the attentional load modulation on a socially meaningful, high-level stimulus.

By applying the attentional load paradigm, our aim is to answer two questions: (1) whether BM would be processed when it is shown away from the focus of attention as a task-irrelevant peripheral stimulus, and (2) if so, whether BM processing would be modulated by attentional load. By answering these questions, we can show (1) if BM is automatically processed in a bottom-up manner in the BM network, even when selective attention is not directed towards it; and (2) whether this bottom-up processing is modulated by a top-down factor that is attentional load. Thus, with this study design, we can examine the interaction between bottom-up and top-down processing of BM in a single task.

2. Methods

2.1. Participants

31 healthy volunteers (23 female; age range 18–31, mean age 23.05) with normal or corrected-to-normal visual acuity and no long-term use of medication for a neurological or psychiatric disorder participated in the study. The study was approved by the Human Research Ethics Committee of Bilkent University in line with The Code of Ethics of The World Medical Association (Declaration of Helsinki). Prior to the experiment, written informed consent and MRI prescreening form of each participant was collected. After the experiment, participants were compensated for their time.

2.2. Stimuli, experimental design and procedure

There were two kinds of stimulus display presented onto the screen: (1) T-shaped stimuli shown at the fovea; (2) Point light displays (PLDs) of intact or scrambled BM stimulus shown at the periphery. All stimuli were generated and presented via the Psychophysics Toolbox (Psychtoolbox Version 3 [PTB-3]; Brainard, 1997; Pelli, 1997; Kleiner et al.,

2007) and BioMotion Toolbox (van Boxtel & Lu, 2013) on MATLAB (The Mathworks, Natick, MA).

The main task consisted of two pseudorandom rapid serial visual presentations (RSVP) of six t-shaped stimuli varying in their color (red, green or yellow) and orientation (upright or upside-down). The task was adapted from previous neuroimaging studies that examined attentional load (Bruckmaier et al., 2020; Desseilles et al., 2009; Rauss, Pourtois, Vuilleumier, & Schwartz, 2012; Schwartz et al., 2004). This RSVP of 12 t-shapes constituted one experimental condition with a duration of 10 s. Each t-shape was displayed for 500 ms and preceded by interstimulus intervals randomly ranging between 250 and 350 ms (Fig. 1.A). The order of t-shapes within the RSVP was pseudorandomized such that the same t-shape would not be displayed in a row. The number of target stimuli (four out of twelve) and overall t-shape displays were kept the same across conditions and blocks. Only the instruction screen (Fig. 1.B) differed based on the attentional load manipulation. Attentional load differed as follows: in the low attentional load instruction, participants were asked to detect red shapes; meanwhile in the high attentional load, they had to detect upright yellow and upside-down green t-shapes. This manipulation is based on the study of Schwartz and colleagues (2004). Accordingly, detecting red shapes depends on the "pop-out" feature of one color among three others; meanwhile, detecting upright yellow or upside-down green t-shapes requires discrimination of a conjunction of color and orientation among all six combinations. Thus, the latter one demands more focused attention compared to the first one.

While participants were engaged in this visual detection task varying in attentional load, either intact or scrambled point-light displays (PLDs) of BM or no stimulus at all were shown 4 visual degrees away from the foveal t-shape stimuli (Fig. 1.C). The total display size of each PLD stimulus was 4,6 × 12,5 visual degrees. The eccentricity and the total display size of peripheral stimuli was optimized for the MR compatible display screen based on Thornton and Vuong's incidental processing of BM study (Thornton and Vuong, 2004) and two previous attentional load studies conducted by Desseilles et al. (2009) who also had portrait positioned task-irrelevant stimuli at the periphery with similar size, and by Schwartz and colleagues (2004) who compared the attentional load modulation on peripheral stimuli at different eccentricities. The PLD animation of a walking human was downloaded from an open motion capture database (CMU Graphics Lab, https://mocap.cs.cmu.edu/) and then edited on Motion Kinematic and Kinetic Analyser software (MOKKA; Barré, 2013, https://biomechanical-toolkit.github.io/mokka/) to acquire a 2D front view with a total of 13 dots comprising a head, shoulders, elbows, hands, waist bones, knees, and feet joint locations. Each animation was reduced to one second and consisted of 61 frames. In order to have the same peripheral stimuli throughout the RSVP of twelve t-shapes, one animation was shown on a total of 10 s-long loop. The scrambled point-light motion stimulus (SCR) was created via Bio-Motion Toolbox (van Boxtel & Lu, 2013) by shuffling the anchor positions of dots in the intact BM stimulus while keeping each dot's local motion trajectories the same. Therefore, SCR had the same number of dots, and the same local dot motion as in intact BM but the global form and motion of the intact BM was disrupted in SCR.

The fMRI experiment consisted of 8 runs. There were four rest and three pairs of experimental blocks in each run. Each run started, ended and was interleaved with rest blocks in which the participant had to fixate on a cross shown at the fovea for 8, 10, 12, or 14 s (11 s on average). The experimental blocks were shown as subsequent pairs (Fig. 1.C) with an instruction screen lasting 5 s prior to their start showing the target stimuli based on the attentional load condition. The order of blocks was counterbalanced. Each experimental block consisted

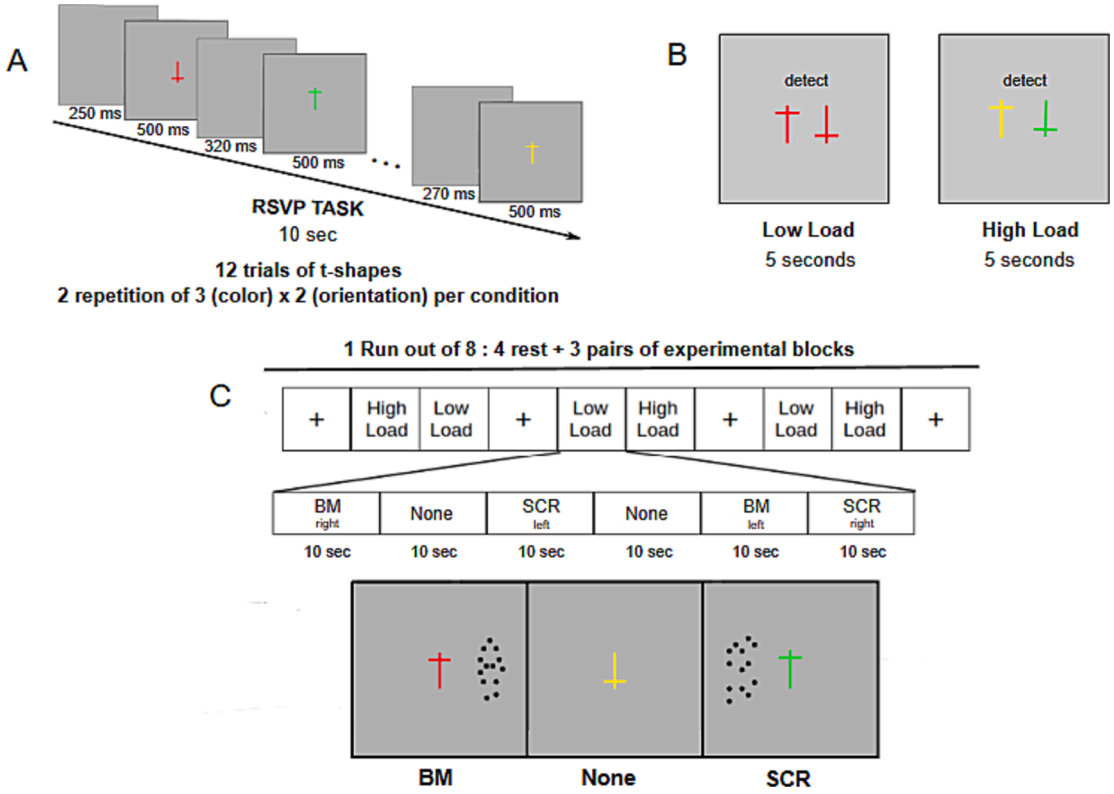

Fig. 1. Stimuli design and procedure. Participants were engaged in a visual detection task at the fovea consisting of (a) Twelve t-shapes varying in their color (i.e. red, green, yellow) and orientation (i.e. upright, upside-down) was shown for 500 ms each with preceding inter-stimulus intervals ranging randomly between 250 and 350 ms. This RSVP task lasted 10 s, constituting one experimental condition. (b) The main stimulus display was the same except for the instruction screen showing the target stimuli. (c) In each run, there were four rest and three pairs of experimental blocks. The display of the main task and the task-irrelevant peripheral stimulus (intact [BM] biological motion, scrambled [SCR] biological motion, or no stimulus at all [None] was shown in the periphery) was kept the same over each experimental block in all runs.

of six peripheral stimulus conditions: BM-right, BM-left, SCR-right, SCR-left, No-peripheral-stimulus condition (None) (Fig. 1.C). The None condition was shown twice to equal the number of conditions within a block. The order of conditions in each experimental block was pseudorandomized such that "None" conditions would not be shown in a row. Furthermore, in order to prevent visual adaptation, intact and scrambled PLDs were shown either right or left side of the screen rather than bilaterally. Overall, each condition had a 10 s-long RSVP task that included 12 trials. In total, there were 72 trials per experimental block constituting 432 trials per run. Each run lasted approximately 7 min 14 s.

Prior to scanning, participants were familiarized with the intact and scrambled BM stimuli separately via an explicit overview of each stimulus, and were tested whether they could discriminate them on the periphery during a fixation on a foveal cross as a separate practice. Lastly, the main task was practiced without any peripheral stimuli for 36 trials per load condition. Once the participants successfully completed the practice trials with a more than 80 % hit rate (Mean number of necessary practice sessions = 1.18; Overall mean hit rate over total number of practice sessions = 80.05 %), they were taken to the scanner room. During the fMRI experiment, they had to detect the target stimuli shown in the instructions as accurately as possible, and they were explicitly told to fixate on the t-shape stimulus and avoid looking at any other stimuli that may appear in the periphery. The stimuli were shown on an MR compatible LED screen (TELEMED, 60 Hz refresh rate, 800 × 600 pixel, 32 in.) and seen via a mirror mounted on the head-coil. Participants' responses were collected via an MR suitable fiber optic button box.

2.3. Behavioral data analysis

A 2 × 3 within-subjects analysis of variance (ANOVA) was conducted (N = 31) to test the effect of attentional load (Attentional Load: High, Low) and peripheral stimulus (PS: BM, SCR, None) on reaction times (RT), accuracy (ACC), and the number of false alarms. For the PS and interaction results in all RT, ACC, and false alarm analyses, Mauchly's test indicated that the assumption of sphericity was violated (RT: PS: $\chi 2$ (2) = 36.973, $p < 0.001$; interaction: $\chi 2$ (2) = 26.959, $p < 0.001$; ACC: PS: $\chi 2$ (2) = 8.605, $p = 0.014$; interaction: $\chi 2$ (2) = 16.579, $p < 0.001$; False alarms: PS: $\chi 2$ (2) = 7.157, $p = 0.028$; interaction: $\chi 2$ (2) = 5.935, $p = 0.051$). Therefore, degrees of freedom for these analyses were corrected using Greenhouse-Geisser estimates of sphericity (RT: PS: $\varepsilon = 0.581$, interaction: $\varepsilon = 0.623$; ACC: PS: $\varepsilon = 0.796$, interaction: $\varepsilon = 0.697$; False alarms: PS: $\varepsilon = 0.821$, interaction: $\varepsilon = 0.051$). Moreover, for the post-hoc comparisons, the Bonferroni correction was applied.

2.4. MRI data acquisition and analyses

Scanning took place at the National Magnetic Resonance Research Center (UMRAM) in Bilkent University with 3 T Siemens TimTrio MR scanner with a 32-channel phase array head coil. In order to minimize head movement, participants' heads were supported with foam padding. Before the experimental scans, high resolution T1-weighted structural images were obtained (TR = 2600 ms, TE = 2.92 ms, flip angle = 12°, FoV read = 256 mm, FoV phase = 87.5 %, 176 slices with 1 × 1 × 1 mm^3 resolution). Then, over eight runs, 227 functional images per run were acquired using gradient-echo planar imaging (TR = 2000 ms, TE = 22 ms, flip angle = 90°, 64 × 64 matrix, FoV read = 192 mm, 43 slices with a thickness of 2.5 mm, 3 × 3 × 2.5 mm^3 resolution).

2.4.1. Anatomical and functional data preprocessing via fMRIPrep

Results included in this study come from preprocessing performed using fMRIPrep 20.1.1 (Esteban, Markiewicz, et al. (2018); Esteban, Blair, et al. (2018); RRID:SCR_016216), which is based on Nipype 1.5.0 (Gorgolewski et al. (2011); Gorgolewski et al. (2018); RRID: SCR_002502).

2.5. Anatomical data preprocessing

A total of 2T1-weighted (T1w) images were found within the input BIDS dataset. All of them were corrected for intensity non-uniformity (INU) with N4BiasFieldCorrection (Tustison et al., 2010), distributed with ANTs 2.2.0 (Avants, Epstein, Grossman, & Gee, 2008, RRID: SCR_004757). The T1w-reference was then skull-stripped with a Nipype implementation of the antsBrainExtraction.sh workflow (from ANTs), using OASIS30ANTs as target template. Brain tissue segmentation of cerebrospinal fluid (CSF), white-matter (WM) and gray-matter (GM) was performed on the brain-extracted T1w using fast (FSL 5.0.9, RRID: SCR_002823, Zhang, Brady, & Smith, 2001). A T1w-reference map was computed after registration of 2 T1w images (after INU-correction) using mri_robust_template (FreeSurfer 6.0.1, Reuter, Rosas, & Fischl, 2010). Brain surfaces were reconstructed using recon-all (FreeSurfer 6.0.1, RRID:SCR_001847, Dale, Fischl, & Sereno, 1999), and the brain mask estimated previously was refined with a custom variation of the method to reconcile ANTs-derived and FreeSurfer-derived segmentations of the cortical gray-matter of Mindboggle (RRID:SCR_002438, Klein et al., 2017). Volume-based spatial normalization to one standard space (MNI152NLin2009cAsym) was performed through nonlinear registration with antsRegistration (ANTs 2.2.0), using brain-extracted versions of both T1w reference and the T1w template. The following template was selected for spatial normalization: ICBM 152 Nonlinear Asymmetrical template version 2009c [Fonov, Evans, McKinstry, Almli, and Collins (2009), RRID:SCR_008796; TemplateFlow ID: MNI152NLin2009cAsym],

2.6. Functional data preprocessing

For each of the 8 BOLD runs found per subject (across all tasks and sessions), the following preprocessing was performed. First, a reference volume and its skull-stripped version were generated using a custom methodology of fMRIPrep. Head-motion parameters with respect to the BOLD reference (transformation matrices, and six corresponding rotation and translation parameters) are estimated before any spatiotemporal filtering using mcflirt (FSL 5.0.9, Jenkinson, Bannister, Brady, & Smith, 2002). BOLD runs were slice-time corrected using 3dTshift from AFNI 20160207 (Cox & Hyde, 1997, RRID:SCR_005927). Susceptibility distortion correction (SDC) was omitted. The BOLD reference was then co-registered to the T1w reference using bbregister (FreeSurfer) which implements boundary-based registration (Greve & Fischl, 2009). Co-registration was configured with six degrees of freedom. The BOLD time-series (including slice-timing correction when applied) were resampled onto their original, native space by applying the transforms to correct for head-motion. These resampled BOLD time-series will be referred to as preprocessed BOLD in original space, or just preprocessed BOLD. The BOLD time-series were resampled into standard space, generating a preprocessed BOLD run in MNI152NLin2009cAsym space. First, a reference volume and its skull-stripped version were generated using a custom methodology of fMRIPrep. Several confounding time-series were calculated based on the preprocessed BOLD: framewise displacement (FD), DVARS and three region-wise global signals. FD was computed using two formulations following Power (absolute sum of relative motions, Power et al. (2014)) and Jenkinson (relative root mean square displacement between affines, Jenkinson et al. (2002)). FD and DVARS are calculated for each functional run, both using their implementations in Nipype (following the definitions by Power et al., 2014). The three global signals are extracted within the CSF, the WM, and the whole-brain masks. Additionally, a set of physiological regressors were extracted to allow for component-based noise correction (CompCor, Behzadi, Restom, Liau, & Liu, 2007). Principal components are estimated after high-pass filtering the preprocessed BOLD time-series (using a discrete cosine filter with 128 s cut-off) for the two CompCor variants: temporal (tCompCor) and anatomical (aCompCor). tCompCor components are then calculated from the top 5 % variable voxels within a mask

covering the subcortical regions. This subcortical mask is obtained by heavily eroding the brain mask, which ensures it does not include cortical GM regions. For aCompCor, components are calculated within the intersection of the aforementioned mask and the union of CSF and WM masks calculated in T1w space, after their projection to the native space of each functional run (using the inverse BOLD-to-T1w transformation). Components are also calculated separately within the WM and CSF masks. For each CompCor decomposition, the k components with the largest singular values are retained, such that the retained components' time series are sufficient to explain 50 percent of variance across the nuisance mask (CSF, WM, combined, or temporal). The remaining components are dropped from consideration. The head-motion estimates calculated in the correction step were also placed within the corresponding confounds file. The confound time series derived from head motion estimates and global signals were expanded with the inclusion of temporal derivatives and quadratic terms for each (Satterthwaite et al., 2013). Frames that exceeded a threshold of 0.5 mm FD or 1.5 standardized DVARS were annotated as motion outliers. All resamplings can be performed with a single interpolation step by composing all the pertinent transformations (i.e. head-motion transform matrices, susceptibility distortion correction when available, and co-registrations to anatomical and output spaces). Gridded (volumetric) resamplings were performed using antsApplyTransforms (ANTs), configured with Lanczos interpolation to minimize the smoothing effects of other kernels (Lanczos, 1964). Non-gridded (surface) resamplings were performed using mri_vol2surf (FreeSurfer).

Many internal operations of fMRIPrep use Nilearn 0.6.2 (Abraham et al., 2014, RRID:SCR_001362), mostly within the functional processing workflow. For more details of the pipeline, see the section corresponding to workflows in fMRIPrep's documentation.

2.7. Univariate analysis and activation maps

After preprocessing, first- and second-level analyses were conducted via SPM12 software package (https://www.fil.ion.ucl.ac.uk/spm/software/spm12/) on MATLAB (The Mathworks, Natick, MA). A design matrix of fourteen regressors (six experimental conditions: BM under High Load [HBM], BM under Low Load [LBM], SCR under High Load [HSCR], SCR under Low Load [LSCR], None under High Load [HNone], None under Low Load [LNone]; one fixation block; six motion regressors: x, y, z solid body translations and x, y, z body rotations; one constant factor) was created for the first-level general linear model (GLM). Each regressor was convolved with the default canonical hemodynamic response function on SPM12. Following the first-level analysis, group level analysis was conducted as a 2 (Attentional load: High, Low) × 3 (PS: BM, SCR, None) within-subject flexible factorial design (Penny, Friston, Ashburner, Kiebel, & Nichols, 2011) with subjects as the independent (i.e. random) factor and six experimental conditions as within-subject (i.e. dependent) factors. T-contrast activity maps for each condition minus fixation is also provided as a supplementary figure (Sup. Fig. 1). All activation maps unless reported otherwise were thresholded at $p < 0.05$ under familywise error (FWE) correction.

2.8. Searchlight-based multivariate pattern analysis (decoding)

In order to discriminate the pattern of brain activity associated with different attentional load modulations (High versus Low) and peripheral stimuli conditions (BM, SCR, None), several decoding analyses were done. Each of six experimental conditions was labeled accordingly in each classification: HBM, HSCR, HNone, LBM, LSCR, LNone. In order to differentiate the pattern of activation in high and low attentional load blocks, "High versus Low" binary classification (Supplementary Fig. 2) was run. Furthermore, three-way (Supplementary Fig. 2) and binary PS classifications were run on PS classes to observe the difference of activation patterns associated with each PS condition: BM versus SCR versus None; BM versus None; SCR versus None; BM versus SCR. Further binary classifications were run in order to discriminate the attentional load modulation on each peripheral stimulus condition to be compared with each other: HBM versus HNone, LBM versus LNone; HSCR versus HNone, LSCR versus LNone; HBM versus HSCR, LBM versus LSCR. Whole-brain decoding maps were created through a searchlight-based (3 mm radius sphere) multivariate pattern analysis (MVPA) with a linear support vector machine (LibSVM; regularization parameter $C = 1$) on the Decoding Toolbox (TDT; Hebart, Görgen, & Haynes, 2015). Runwise beta images were extracted from the first-level GLM of each subject and used as inputs for the classifiers. Leave-one-run-out cross-validation procedure was applied and the accuracy minus chance brain images of each subject were created to be used in the one-sample *t*-test group analysis. The applied threshold was at $p < 0.05$ under FWE correction.

3. Results

3.1. Behavioral results

3.1.1. Accuracy

The task was completed successfully by participants as indicated by an overall accuracy being more than 80 percent. Accuracy was inferred from the hit rate analysis which calculates the number of hits divided by the total number of hits, false alarms, and missed trials per condition. Accordingly, an accuracy of one hundred would mean that the participant has responded correctly to all target trials with no missed and false alarm response. There was a main effect of attentional load ($F(1,30) = 85.307$, $p < 0.001$, $\eta^2 = 0.671$). The accuracy rate in the low load ($M = 0.97$, $SD = 0.03$) was significantly higher than that of high load ($M = 0.84$, $SD = 0.081$) ($t(30) = 9.236$, $p_{bonf} < 0.001$). However, there was no main effect of PS (($F(1,30) = 1.231$, $p = 0.299$), and no interaction between the load and the PS conditions (($F(1,30) = 2.071$, $p = 0.135$). The results showed that regardless of the PS, the attentional load effect was evident on the accuracy rates.

In terms of the number of false alarms, there was a significant main effect of attentional load ($F(1,30) = 91.377$, $p < 0.001$, $\eta2 = 0.501$) and PS ($F(1,30) = 77.223$, $p < 0.001$, $\eta2 = 0.145$). The number of false alarms in the high load blocks was significantly higher than that of low load ($t(30) = 9.559$, $p_{bonf} < 0.001$). Moreover, post hoc results on PS conditions showed that the number of false alarms in the BM and SCR conditions separately was significantly higher than that of no PS condition (BM > None: $t(30) = 11.365$, $p_{bonf} < 0.001$; SCR > None: $(30) = 10.037$, $p_{bonf} < 0.001$). There was no significant difference between BM and SCR conditions ($t(30) = 1.328$, $p_{bonf} = 0.568$). Furthermore, the number of false alarms among PS conditions in the low load was not significantly different from each other (LBM > LSCR: $t(30) = 0.032$, $p_{bonf} = 1$; LBM > LNone: $t(30) = 1.787$, $p_{bonf} = 1$; LSCR > LNone: $t(30) = 1.755$, $p_{bonf} = 1$), either. Overall, the results were in two-folds: firstly, although there was no significant difference among PS conditions in terms of accuracy rates, participants made more false alarms when there was a peripheral stimulus in the periphery indicating that the PS did not decrease the number of hits but increased the number of false alarms; secondly, false alarms were higher in the high load than low load blocks indicating the attentional load modulation on not only accuracy rates but also false alarms.

3.1.2. Reaction times

Reaction time (RT) analysis showed that there was a main effect of attentional load ($F(1,30) = 82.507$, $p < 0.001$, $\eta^2 = 0.33$) and PS ($F(1,30) = 115.956$, $p < 0.001$, $\eta^2 = 0.273$) (Table 1). The RTs found in the high load was significantly higher than that of low load ($t(30) = 9.083$, $p < 0.001$). Post-hoc tests on the PS conditions showed that participants' RTs during no PS condition was significantly higher than that of BM ($t(30) = 12.976$, $p_{bonf} < 0.001$) and SCR ($t(30) = 13.391$, $p_{bonf} < 0.001$) conditions. While the RTs in intact and scrambled BM conditions were

Table 1
Reaction Times Analysis Results.

Cases	Sphericity Correction	Sum of Squares	df	Mean Square	F	p	η^2	η_p^2
Load	None	0.074	1	0.074	82.507	<0.001	0.33	0.733
Residuals	None	0.027	30	$8.962e^{-4}$				
Peripheral Stim	None	0.061[a]	2[a]	0.031[a]	115.956[a]	<0.001[a]	0.273	0.794
	Greenhouse-Geisser	0.061	1.162	0.053	115.956	<0.001	0.273	0.794
Residuals	None	0.016	60	$2.635e^{-4}$				
	Greenhouse-Geisser	0.016	34.873	$4.533e^{-4}$				
Load * Peripheral Stim	None	0.038[a]	2[a]	0.019[a]	134.214[a]	<0.001[a]	0.168	0.817
	Greenhouse-Geisser	0.038	1.246	0.030	134.214	<0.001	0.168	0.817
Residuals	None	0.008	60	$1.402e^{-4}$				
	Greenhouse-Geisser	0.008	37.376	$2.251e^{-4}$				

Note. Type III Sum of Squares.
a: Mauchly's test of sphericity indicates that the assumption of sphericity is violated ($p < 0.05$).
η_p^2: Partial eta squared.

not significantly different from each other ($t(30) = 0.414$, $p_{bonf} = 1$).

Moreover, a significant interaction between the load and PS was also found ($F(1,30) = 134.214$, $p < 0.001$, $\eta 2 = 0.168$). Post-hoc tests on each of six conditions revealed that although there was a significant difference between SCR and None (HSCR > HNone: $t(30) = -19.490$, $p_{bonf} < 0.001$) as well as BM and None conditions (HBM > HNone: $t(30) = -18.497$, $p_{bonf} < 0.001$), SCR and BM conditions did not significantly differ from each other under the high load (HBM > HSCR: $t(30) = 0.993$, $p_{bonf} = 1$). None of the pair-wise PS comparisons were significantly different from each other under low attentional load comparisons (Table 2).

3.2. Whole-brain univariate activation maps

In order to examine the whole-brain activity maps during the bottom-up perception of BM, we have conducted whole-brain within-subject flexible factorial (FF) analysis. All results are thresholded at FWE-corrected, $p < 0.05$; and the peak-level results are reported.

3.2.1. Main effect of attentional load

The main effect of attentional load as indicated by an F-test on high and low attentional load blocks yielded two different response maps in regions within the fronto-parietal attention network during high load, and those within default mode network (DMN) during low load (Table 3, Fig. 2.a).

Further t-contrast analysis revealed that for the High > Low contrast, in line with the literature (Chong, Williams, Cunnington, & Mattingley, 2008; Desseilles et al., 2009; Schwartz et al., 2004), significant activation was found within the left inferior parietal lobule (peak: −25 −70 42; T = 10.23) and left superior frontal gyrus (peak: −31 −4 69; T = 9.32) that constitute the fronto-parietal attention network (Fig. 2.b).

Table 2
Post Hoc Comparisons - Load * Peripheral Stim.

		Mean Difference	SE	t	p_{bonf}
High, BM	Low, BM	0.022	0.005	4.409	<0.001
	High, SCR	0.004	0.004	0.993	1
	Low, SCR	0.021	0.005	3.883	0.004
	High, None	−0.067	0.004	−18.497	<0.001
	Low, None	0.013	0.005	2.452	0.255
Low, BM	High, SCR	−0.019	0.005	−3.437	0.016
	Low, SCR	−0.001	0.004	−0.323	1
	High, None	−0.089	0.005	−16.435	<0.001
	Low, None	−0.009	0.004	−2.469	0.226
High, SCR	Low, SCR	0.017	0.005	3.465	0.017
	High, None	−0.070	0.004	−19.490	<0.001
	Low, None	0.01	0.005	1.79	1
Low, SCR	High, None	−0.088	0.005	−16.219	<0.001
	Low, None	−0.008	0.004	−2.146	0.512
High, None	Low, None	0.08	0.005	15.908	<0.001

Note. P-value adjusted for comparing a family of 15.

Table 3
Main effect of attentional load. Results were FWE-corrected, at a threshold of $p < 0.05$.

Main Effect of Attentional Load		
Region	*Coordinates*	*F-Score*
L Precuneus	−4 −55 19	127.55
L Angular Gyrus (IPL) (BA23)	−46 −79 37	115.7
L Middle Orbital Gyrus (BA39)	−1 60 −11	108.52
L Inferior Parietal Lobule (BA39)	−25 −70 42	104.65
L Superior Frontal Gyrus (BA6)	−31 −4 69	86.81
L Posterior Medial Frontal (BA6)	−4 9 52	81.87
R Middle Occipital Gyrus (BA7)	30 −67 32	85.15
R Angular Gyrus (IPL) (BA39)	51 −73 34	74.16
R Middle Frontal Gyrus (BA6)	27 −7 49	69.01
High > Low		
Region	*Coordinates*	*T-Score*
L Inferior Parietal Lobule (BA39)	−25 −70 42	10.23
L Superior Frontal Gyrus (BA6)	−31 −4 69	9.32
L Posterior Medial Frontal (BA6)	−4 9 52	9.05
R Middle Occipital Gyrus (BA7)	30 −67 32	9.23
R Insula Lobe (BA45)	33 24 9	8.65
R Middle Frontal Gyrus (BA6)	27 −7 49	8.31
Low > High		
Region	*Coordinates*	*T-Score*
L Precuneus (BA23)	−4 −55 19	11.29
L Angular Gyrus (IPL) (BA39)	−46 −79 37	10.76
L Middle Orbital Gyrus (BA10)	−1 60 −11	10.42
R Angular Gyrus (IPL) (BA39)	51 −73 34	8.61

Additionally, posterior medial frontal gyrus in the left hemisphere that is associated with error-monitoring and post-error adjustments (Danielmeier, Eichele, Forstmann, Tittgemeyer, & Ullsperger, 2011) were found activated (peak = -4 9 52; T = 9.05). For the Low > High t-contrast, DMN regions (Raichle, 2015) were observed (Fig. 2.c), revealing activity maps in left precuneus (peak: −4 −55 19; T = 11.29), left and right angular gyri (peak: −46 −79 37; F = 10.76) (peak: 51 −73 34; T = 8.61), and left middle orbital gyrus (peak = -1 60 −11; T = 10.42) (Table 3).

3.2.2. Main effect of peripheral stimulus

The main effect of PS as indicated by an F-test on BM, SCR, and None conditions yielded bilateral activity maps in secondary visual (BA18) and visual association (BA19) cortices including motion sensitive MT/V5 region as expected (Fig. 3.a, Table 4).

Furthermore, separate comparisons between each PS and None conditions yielded similar activities for both BM > None and SCR > None t-contrasts (Table 4): bilateral secondary visual (BA18) and visual

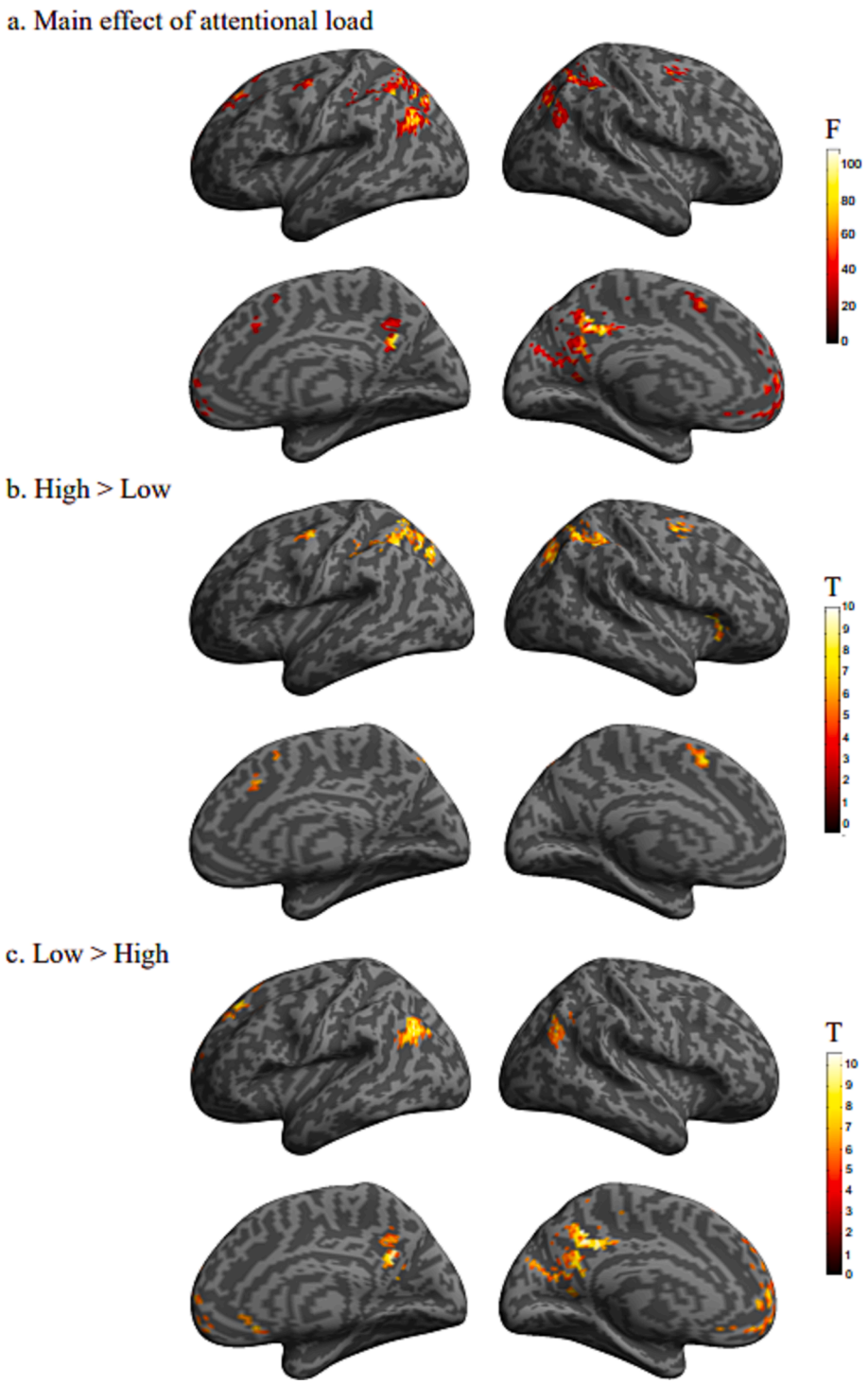

Fig. 2. Univariate activation maps for attentional load. (a) The activity maps of the main effect of attentional load. The F-test results showed fronto-parietal attention and DMN region activations. (b) The activity maps of the High > Low attentional load t-contrast. The t-contrast of High > Low showed fronto-parietal network activation. (c) The activity maps of the Low > High attentional load t-contrast. The t-contrast of Low > High showed activation within DMN. Results were FWE-corrected, at a threshold of $p < 0.05$.

association (BA19) cortices including motion-sensitive MT/V5 regions were activated in both contrasts (Fig. 3.b).

Overall, the bottom-up processing of PS was observed in motion-sensitive visual areas regardless of the attentional load. Contrary to our expectation, there was no difference between intact and scrambled BM stimuli indicating more general response towards the dynamic stimulus that is not specific to BM.

3.2.3. *Attentional load modulation on peripheral stimulus*

Attentional load modulation on PS is indicated by the decreased activation or diminished activity maps in high load blocks as compared to low load blocks. Accordingly, while there was a significant activation found within the OTC regions towards the BM > None and SCR > None contrasts under low load, only an early visual cortex region showed activity towards the same contrasts under high load (Table 5).

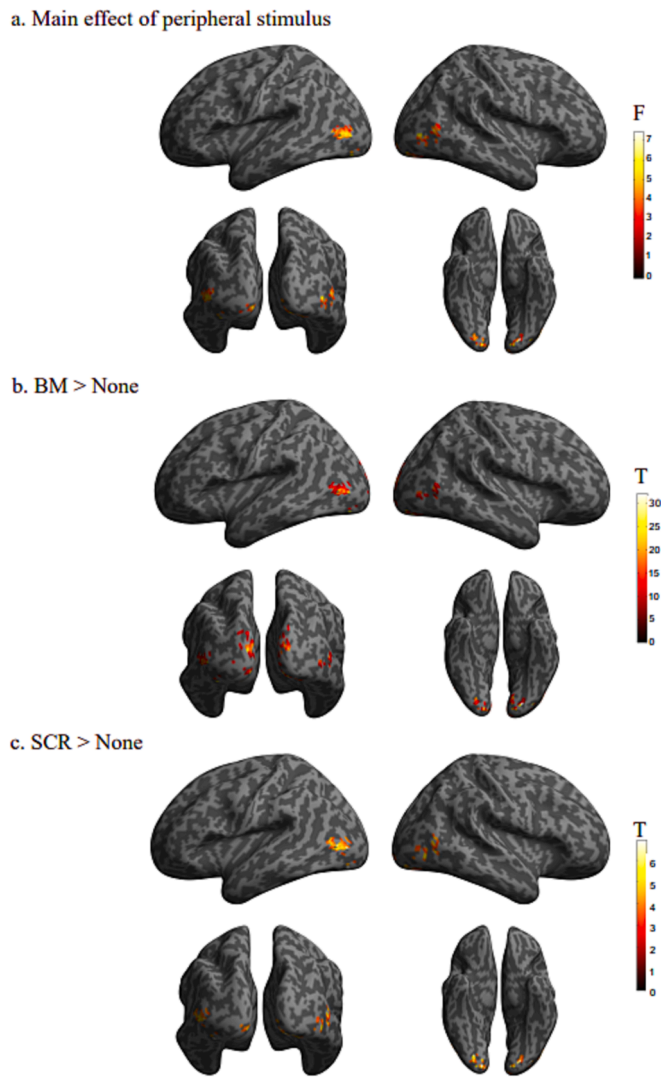

Fig. 3. Univariate activation maps for peripheral stimulus. (a) The activity maps of the main effect of peripheral stimulus. The F-test results showed activity maps in medial early visual cortex and motion-sensitive regions in the OTC. (b) The activity maps of the BM > None t-contrast. The t-contrast of BM > None showed activation at motion-sensitive regions in the OTC. (c) The activity maps of the SCR > None t-contrast. The t-contrast of SCR > None yielded activation at motion-sensitive regions in the OTC. For the purpose of visualization, results are shown at an uncorrected threshold of $p < 0.001$.

3.3. Whole-brain searchlight based MVPA

Considering the increased sensitivity of multivariate pattern analysis compared to univariate analysis (Davis et al., 2014), we conducted a searchlight based MVPA on the whole-brain to test which brain regions could discriminate between the processing of each PS condition under high and low attentional load. The group-level one sample *t*-test results on chance minus accuracy brain images of each participant was calculated for the following binary classifications: BM vs None, LBM vs LNone, HBM vs HNone, SCR vs None, LSCR vs LNone, HSCR vs HNone.

3.3.1. BM vs None classification results

Regardless of the attentional load block, motion and form sensitive regions in OTC could significantly decode BM and None conditions (Fig. 4.a). The attentional load modulation was evident as indicated by the diminished extent and amount of the regions that could discriminate between the BM and None classes under the high load as compared to low load (Fig. 4.b and Fig. 4.c). Specifically, the decoding regions for BM vs None were at peak in the bilateral middle occipital gyrus (Left: peak: −46 −82 4; T = 9.92; Right: peak: 42 −73 4; T = 7) and left lingual gyrus (peak: −16 −88 −14; T = 15.4). For the same comparison under low attentional load, the regions that could significantly separate LBM and

Table 4
Main effect of peripheral stimulus. Results with asterisks are at the FWE-corrected $p < 0.05$ threshold, the rest is at an uncorrected threshold of $p < 0.001$.

Main Effect of Peripheral Stimulus		
Region	*Coordinates*	*F-Score*
L Lingual Gyrus (BA18)**	−19 −88 −11	32.3
L Middle Occipital Gyrus (BA19)**	−46 −73 9	31.41
L Superior Occipital Gyrus (BA18)**	−10 −100 14	27.59
L Inferior Occipital Gyrus (BA18)**	−31 −82 −11	25.88
R Lingual Gyrus (BA18)**	21 −88 −9	29.44
R Middle Occipital Gyrus (BA19)	54 −76 2	27.38
BM > None		
Region	*Coordinates*	*T-Score*
L Lingual Gyrus (BA18)**	−19 −88 −11	7.44
L Middle Occipital Gyrus (BA19)**	−52 −82 7	7.41
L Inferior Occipital Gyrus (BA18)**	−28 −85 −11	6.26
R Middle Occipital Gyrus (BA19)	54 −76 2	7.01
R Lingual Gyrus (BA18)	15 −91 −14	6.85
SCR > None		
Region	*Coordinates*	*T-Score*
L Inferior Occipital Gyrus (BA18)**	−31 −82 −11	6.79
L Middle Occipital Gyrus (BA19)**	−46 −73 9	6.55
L Lingual Gyrus (BA18)	−19 −88 −11	6.53
R Lingual Gyrus (BA18)**	21 −88 −9	7.17
R Middle Occipital Gyrus (BA19)	54 −76 2	5.73
BM > SCR		
No activity		

Table 5
Attentional load modulation on peripheral stimulus. Results with asterisks are at the FWE-corrected $p < 0.05$ threshold, the rest is at an uncorrected threshold of $p < 0.001$.

Low-BM > Low-None		
Region	*Coordinates*	*T-Score*
L Middle Occipital Gyrus (BA19)**	−46 −73 9	7.14
L Lingual Gyrus (BA18)	−19 −88 −11	6.34
L Inferior Occipital Gyrus (BA18)	−28 −85 −11	6.1
R Middle Occipital Gyrus (BA19)	54 −76 2	6.76
High-BM > High-None		
Region	*Coordinates*	*T-Score*
R Lingual Gyrus (BA18)	15 −91 −14	5.24
Low-SCR > Low-None		
Region	*Coordinates*	*T-Score*
L Middle Occipital Gyrus (BA19)**	−52 −76 7	6.69
L Inferior Occipital Gyrus (BA18)	−31 −82 −11	6.43
L Middle Occipital Gyrus (BA19)	−43 −82 2	5.65
R Fusiform Gyrus (BA18)	27 −79 −6	6.44
R Lingual Gyrus (BA18)	21 −88 −9	6.26
R Middle Temporal Gyrus (BA37)	51 −73 2	6.08
High-SCR > High-None		
Region	*Coordinates*	*T-Score*
L Calcarine Gyrus (BA18)	−4 −94 −6	5.42
L Lingual Gyrus (BA18)	−19 −88 −11	5

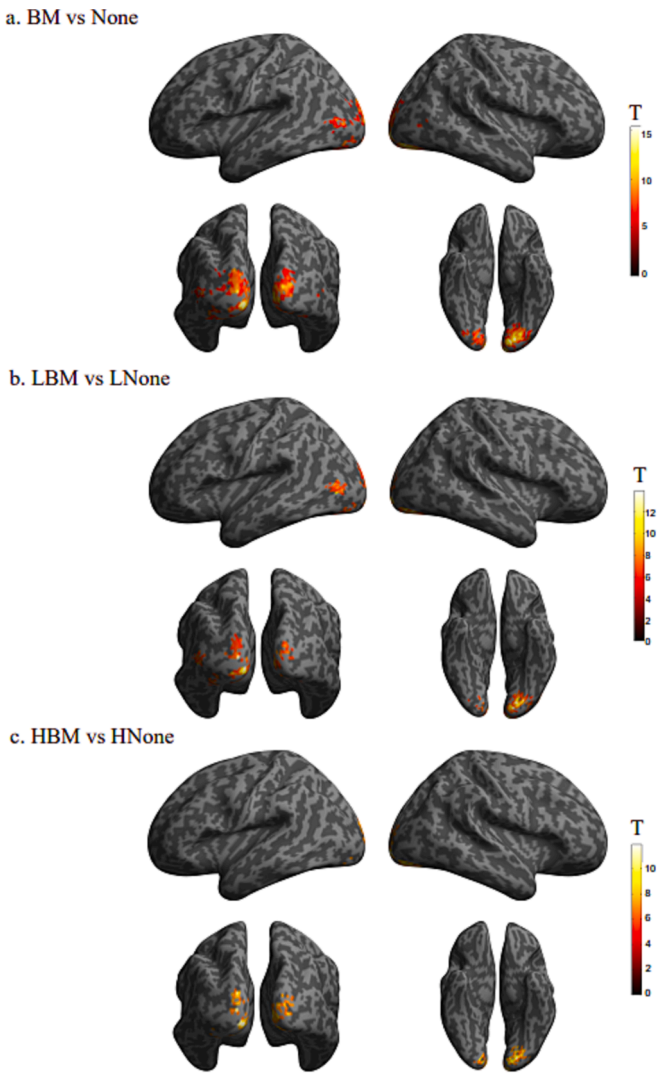

Fig. 4. Multivariate pattern analysis results of the attentional load modulation on intact BM stimuli. (a) Decoding regions of the BM versus None classification: Motion and form sensitive OTC regions were shown to discriminate BM and None conditions regardless of the attentional load. (b) Attentional load modulation on BM was evident: Under low attentional load, BM and None could be decoded in the OTC regions; while (c) under high load, only the early visual areas could discriminate BM and None stimuli. Results were FWE-corrected, at a threshold of $p < 0.05$.

LNone classes included calcarine gyrus (peak: −13 −97 −4; T = 15.51) and middle occipital gyrus (peak: −49 −79 2; T = 10.5) in the left hemisphere, in addition to the lingual gyrus (peak: 24 −85 −14; T = 7.13) in the right hemisphere. As expected, due to the modulation of attentional load, the same comparison under high load showed only calcarine gyrus in the left hemisphere (peak: −10 −91 −4; T = 13.59) as the region that significantly separates HBM and HNone from each other (Table 6).

3.3.2. SCR vs None classification results

The SVM could discriminate between the SCR and None conditions over all attentional load blocks at the motion and form sensitive OTC regions (Fig. 5.a). The modulation of attentional load was evident as indicated by the decreased amount and extension of decoding regions in the high load as compared to that of low load (Fig. 5.b and Fig. 5.c). Specifically, regardless of the attentional load block, SCR versus None classification could be decoded at fusiform gyrus (peak: −22 −82 −11; T = 14.32) and middle occipital gyrus (peak: −49 −76 14; T = 9.38; peak: −31 −70 −6; T = 6.79) in the left hemisphere. Moreover, under the low load, SCR and None conditions could be discriminated significantly at the calcarine gyrus (peak: −10 −94 −4; T = 12.13), superior occipital gyrus (peak: −19 −97 17; T = 9.06), and middle occipital gyrus (peak: −52 −82 4, T = 7.12) regions in the left hemisphere. Under high load, the same comparison of SCR and None conditions yielded peak coordinates at calcarine (peak: −7 −91 −6, T = 14.85) and superior occipital gyrus (peak: −13 −97 19, T = 9.28) regions in the left hemisphere (Table 6).

Table 6
Attentional load modulation on BM indicated by the diminished extent of decoding regions. Results were FWE-corrected, at a threshold of $p < 0.05$.

BM vs None		
Region	*Coordinates*	*T-Score*
L Lingual Gyrus (BA18)	−16 −88 −14	15.4
L Middle Occipital Gyrus (BA19)	−46 −82 4	9.92
R Middle Occipital Gyrus (BA19)	42 −73 4	7
Low-BM vs Low-None		
Region	*Coordinates*	*T-Score*
L Calcarine Gyrus (BA18)	−13 −97 −4	15.51
L Middle Occipital Gyrus (BA19)	−49 −79 2	10.5
R Lingual Gyrus (BA19)	24 −85 −14	7.13
High-BM vs High-None		
Region	*Coordinates*	*T-Score*
L Calcarine Gyrus (BA18)	−10 −91 −4	13.59
SCR vs None		
Region	*Coordinates*	*T-Score*
L Fusiform Gyrus (BA18)	−22 −82 −11	14.32
L Middle Occipital Gyrus (BA19)	−49 −76 14	9.38
L Middle Occipital Gyrus (BA19)	−31 −70 −6	6.79
Low-SCR vs Low-None		
Region	*Coordinates*	*T-Score*
L Calcarine Gyrus (BA18)	−10 −94 −4	12.13
L Superior Occipital Gyrus (BA18)	−19 −97 17	9.06
L Middle Occipital Gyrus (BA19)	−52 −82 4	8.67
L Middle Occipital Gyrus (BA19)	−40 −88 4	7.12
High-SCR vs High-None		
Region	*Coordinates*	*T-Score*
L Calcarine Gyrus (BA18)	−7 −91 −6	14.85
L Superior Occipital Gyrus (BA18)	−13 −97 19	9.28
L Superior Occipital Gyrus (BA18)	−13 −97 29	6.91

4. Discussion

In this study, the bottom-up processing of biological motion under the top-down modulation of attentional load was measured in order to see whether such socially and ecologically important stimuli as BM would be processed in the BM network even when it was shown away from the focus of attention and if so whether this processing would be modulated by a top-down factor that is attentional load.

In line with the previous literature on attentional load, the task-irrelevant PS (i.e. intact and scrambled BM stimuli) were found to be incidentally processed within the brain. Accordingly, for both PS conditions, we found an activation within the motion-sensitive OTC regions (i.e. hMT+). However, this activation was not specific to BM itself as we did not find any difference between BM and SCR conditions unlike the Flanker study results by Thornton and Vuong (2004). Yet, in line with our expectations, this bottom-up processing to the motion stimuli was

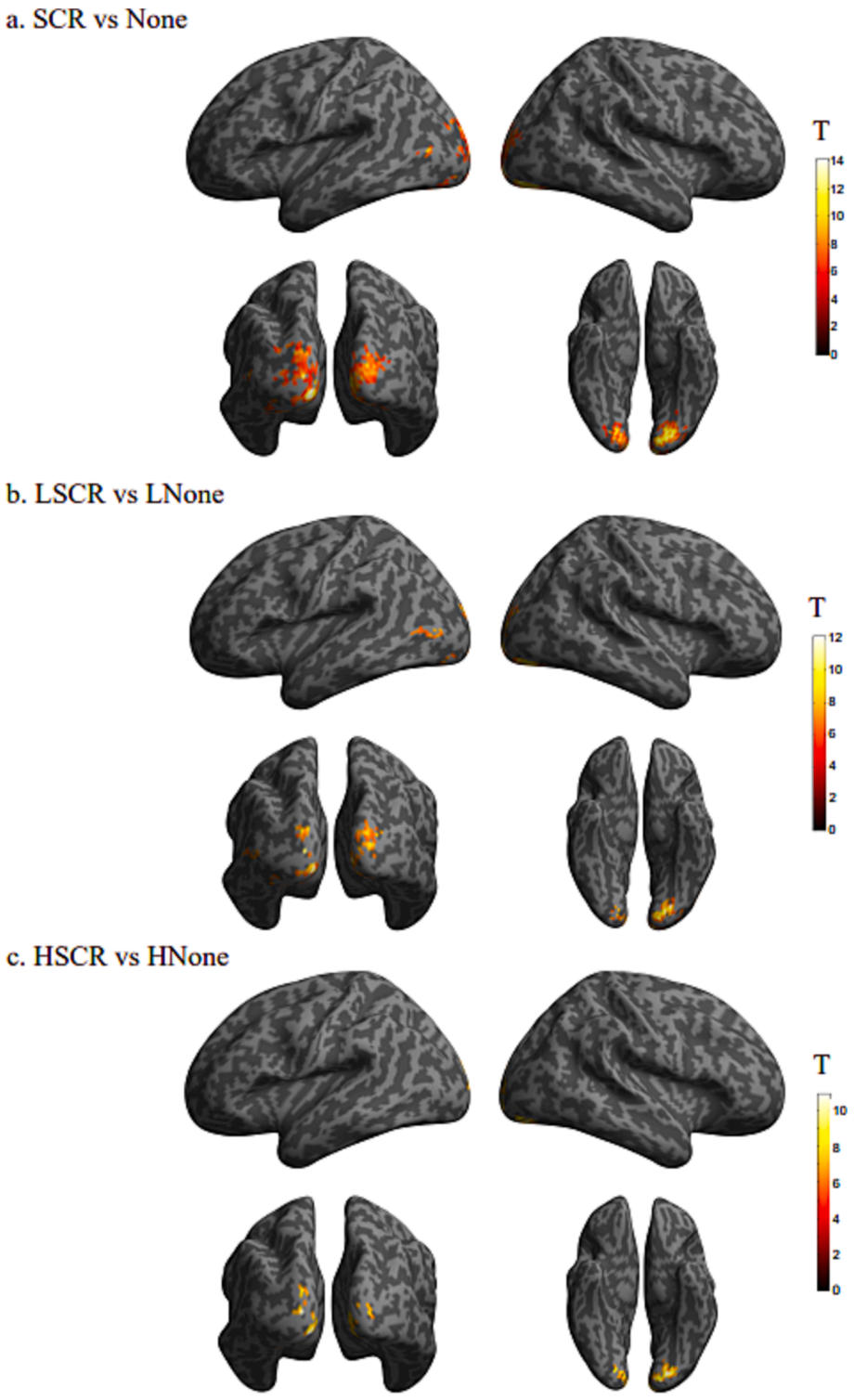

Fig. 5. Multivariate pattern analysis results of the attentional load modulation on scrambled BM stimuli. (a) Decoding regions of the SCR versus None classification: Motion sensitive regions in OTC could discriminate SCR and None conditions regardless of the attentional load. (b) Attentional load modulation on SCR was evident: Under low attentional load, SCR and None could be decoded in the motion sensitive OTC regions; while (c) under high load, only the early visual areas could discriminate SCR and None stimuli. Results were FWE-corrected, at a threshold of $p < 0.05$.

modulated by attentional load as indicated by the decreased activation and diminished decoding regions observed in hMT+under high load. Further details regarding the bottom-up perception of PS and the promise of using the attentional load paradigm in BM literature is discussed below.

4.1. The bottom-up perception of BM

The literature on neural processing of BM under selective attention shows three core brain areas (Thompson & Parasuraman, 2012): (1) The OTC including form and motion sensitive regions (i.e. EBA, FBA, hMT+) as well as STS; (2) parietal (i.e. IPS, IPL); and (3) frontal regions (i.e. IFG,

PMC). However, there are inconsistent results in terms of the regions that are associated with the incidental, bottom-up processing of BM (Herrington et al., 2012; Jastorff & Orban, 2009; Saygin & Sereno, 2008).

In the current study, we found that regardless of the attentional load, OTC regions including motion sensitive areas were activated during the bottom-up perception of both intact and scrambled BM stimuli. These regions were evident specifically under low attentional load. However, under high attentional load, the activation was constrained to the early visual cortex regions indicating the attentional load modulation on PS. This finding is in line with the previous attentional load studies by showing attentional load modulation on the task-irrelevant stimuli in the periphery. However, unlike in the study of Thornton and Vuong (2004), this incidental processing of the PS was not specific to intact BM. In the aforementioned study, Thornton and Vuong (2004) measures the flanker effect of task-irrelevant to-be-ignored BM stimuli in the periphery while (i) manipulating the eccentricity of BM stimuli, (ii) scrambling the BM stimuli, and (iii) making the BM's walking direction ambiguous. Among these conditions, the flanker effect was significantly evident only in the presence of intact BM across all eccentricities (from 1.78 to 4.86 visual degrees) rather than the presence of scrambled or ambiguous BM stimuli. Based on this finding we also expected to find a difference between BM and SCR conditions under attentional load. However, although attentional load modulation significantly affected both PS conditions, the activation maps and patterns were similar between the two. Thus, the incidental processing of the PS was not specific to BM stimulus itself but rather to a more general dynamic nature of the stimulus.

This unexpected finding could be related to two points. Firstly, in terms of the recruited brain regions, there was no significant activation found within the pSTS. In the literature, there are inconsistent results towards the neural correlates of bottom-up BM perception. Some studies found activation only in EBA and hMT+ (Herrington et al., 2012; Jastorff & Orban, 2009), while some found additional activity in STS and IPS (Saygin & Sereno, 2008). This discrepancy between results led us to exploratively hypothesize that under low attentional load, we could see activity maps in not only motion- and form-sensitive areas of OTC, but also in pSTS and parietal cortex. However, our results were constrained to the motion-sensitive OTC regions (i.e. hMT+) and were not specific to the BM itself. This finding could be due to the main methodological difference between our study and the study that found pSTS and IPS activity: The stimulus set. In Saygın and Sereno's retinotopy study (2008), participants' field of view was populated by intact and scrambled BM stimuli. Meanwhile, in our study and studies of those that did not find pSTS activity (Herrington et al., 2012; Jastorff & Orban, 2009), only one action (i.e. walking) of a single BM PLD stimulus was shown on the screen throughout the experiment. Thus, the increased number of stimuli, as well as the contrasting nature of the simultaneous display of intact and scrambled PLDs covering the whole field of view might have resulted in stronger stimulation in the BM processing brain regions. Therefore, the possible reason why we did not see pSTS activity and BM specific incidental processing in our study could be the use of one PLD of BM stimulus that is not strong enough to yield activation beyond motion-sensitive areas in the OTC and therefore fails to show a modulation specific to intact rather than scrambled BM.

The unsuccessful forming of BM representation indicated by the lack of pSTS activation could also be linked to BM recognition. The previous literature showed that abstract action representation based on BM stimulus is formed in the pSTS. Moreover, Grossman, Blake, and Kim (2004) have found that pSTS activation directly depended on participants' ability to recognize PLDs as BM. In their perceptual learning study, only when participants could recognize the PLDs of BM stimulus under the noise mask, the pSTS activation was observed. Thus, it could be that our participants could not recognize the PLDs as BM and in turn we neither found difference between intact and scrambled BM stimuli, nor any significant pSTS activation. However, considering the successful completion of participants on a small task conducted prior to the MR scanning in which participants indicated where the intact, not the scrambled, BM was shown on the laptop screen; this conclusion may be unlikely. It would be interesting to replicate our study with a similar stimulus set of Saygin and Sereno (2008) and compare whether pSTS activity and difference between intact and scrambled BM would be observed.

4.2. Engagement of top-down and bottom-up attention networks

In addition to the bottom-up processing of BM as indicated by the main effect of peripheral stimuli, we have also found a main effect of attentional load evident in brain areas that are part of different attention network regions. In this study, participants had to direct their attention towards a main visual detection task that was shown at the fovea, while ignoring the task-irrelevant peripheral stimulus. Although the display of the foveal task was kept the same across experimental blocks, the attentional load of the main task was manipulated via increasing the demand of attention resources towards the main task. For the high load task, participants had to detect a conjunction of orientation and color (i.e. upright yellow and upside green t-shapes) rather than a pop-out feature of the t-shape (i.e. color: red shapes). Detecting the conjunction targets rather than the pop-out singleton required participants to focus on the foveal task more than the other (Schwartz et al., 2004). Accordingly, the high load task demanded more attention as compared to low load task. Thus, in line with the previous literature (Schwartz et al., 2005; Desseilles et al., 2009), during the High > Low load contrast (Fig. 2.b) as well as the High versus Low load classification (Supplementary Fig. 1), we found the fronto-parietal network (FPN) regions indicating increased demand of attentional engagement towards the high load task.

Interestingly, in the Low > High attentional load contrast, we found activation in the default-mode network (DMN) regions. This is the very first evidence to see the interaction between DMN and FPN in an attentional load paradigm. In the working memory literature, it has been shown repeatedly that the DMN activity follows two distinct mechanisms. Firstly, it gets activated during the baseline state in which the participant is not involved in any cognitive task or is engaged in mind-wandering. Secondly, it deactivates during cognitively or attentionally demanding tasks that we see often in the working-memory literature such as performing arithmetics, recalling a set of strings or numbers, or similar to our study, giving response towards a predetermined target (Jenkins, 2019; Arsalidou et al., 2013; Corbetta, Patel & Schulman, 2008).

When we analyzed the DMN and FPN regions' activation in High > Low and Low > High contrasts, we found that for the High > Low contrast, there is a significant activation in FPN with a deactivation in DMN regions; and the opposite is correct for the Low > High contrast (Supplementary Fig. 4). This finding is in line with the triple network model that was proposed by Menon (2011), in which as the FPN gets activated DMN regions show deactivation; and vice versa (Lesage & Stein, 2016). Although it was not the aim of this current study to examine the attention networks in depth, one might have expected to see the ventral attention network (VAN, saliency network) rather than the DMN. VAN is the third network in this triple model which is associated with the stimulus-driven processing of the unexpected, task-irrelevant stimuli (Menon, 2011). The possible reason why we did not observe VAN activity during peripheral stimuli conditions could be that the biological motion stimulus shown at the periphery was not an unexpected event (Corbetta, Kincade, Ollinger, McAvoy, & Shulman, 2000). The amount of trials and the repetition of peripheral stimulus blocks were equal to each other. Also, before the study started, participants were familiarized with the BM stimuli and they were explicitly told that they may see to-be-ignored intact or scrambled BM stimuli at the periphery.

In sum, this is the very first study in the field of attentional load that

shows the interplay between DMN and FPN regions. It is not surprising for us to find such a relationship, since in addition to the no-peripheral stimulus baseline condition, we also used a control stimulus (i.e. scrambled motion). This has led us to discriminate the attentional load modulation on the BM stimulus from the distinct brain regions that are associated with low and high attentional load tasks while being able to compare them separately.

4.3. Speed-accuracy trade-off present in behavioral results

In addition to the neuroimaging results discussed above, behavioral results also revealed that the attentional load effect was evident on each PS condition. Participants responded faster when there was a task-irrelevant stimulus (BM or SCR) in the periphery as compared to nothing during high attentional load; but there was no difference between the intact and scrambled BM conditions in neither high nor low attentional load blocks. Although this finding seems counterintuitive, the false alarm increase during PS presence may show a speed-accuracy trade-off strategy among participants. Because of the block design nature of the current fMRI study for better signal detection, the duration of conditions (thus, the display duration of PS stimuli) was similar to previous attentional load fMRI studies with meaningless peripheral stimulus (20 s presentation of flickering checkerboard display: Schwartz et al., 2005; and Mondrian-like color patches: Desseilles et al., 2009); while significantly longer than behavioral attentional capture studies with task-irrelevant but semantically meaningful stimuli that report the opposite pattern of performance for RT (Forster & Lavie, 2008: 100 ms cartoon characters; Lleras, Chu, & Buetti, 2017: 200 ms of cartoon characters and object images). Considering the more than 80 % of accuracy in both attentional load conditions and being explicitly told to ignore the task-irrelevant PS stimuli, participants could have developed a strategy to give faster response when they noticed something in their periphery to stick to the instruction while they were more relaxed and unconstrained to perform their task without the presence of PS in their periphery. This could have led to faster RT but more false alarms during PS presence as compared to PS absence trials especially when the task was more demanding (i.e. High load).

4.4. Limitations

In the literature, diminished activation of the task-irrelevant peripheral stimuli has been an indicator of the attentional load modulation. One may suggest that the relatively stronger and extensive activation observed in the low load blocks may be due to the unintentional shift in the eye gaze towards the peripheral stimulus. This possibility could be relevant for our study as well. Considering the early preference and recognition ability of humans towards BM stimuli, one may argue that participants might have shifted their eye gaze towards the peripheral BM stimulus unintentionally. Such shifts in the eye-gaze would yield activity maps similar to the perception of BM under selective attention. However, we did not find any region beyond OTC that could explain the involuntary eye-gaze towards the BM stimulus. So, although we did not use eye-tracker to check whether participants' eye gaze shifted away from the fixation task, our results show no sign of active viewing of peripheral BM stimuli even under low attentional load.

4.5. Future directions

Our study shows that the use of the attentional load paradigm is promising to study the bottom-up processing of BM to develop further the model by Giese and Poggio (2003). Accordingly, in their model, there are two separate but parallel processes representing the form and motion pathways. Each pathway consists of an increasing hierarchy of neural feature detectors with increasing receptive field sizes and complexity. The significance of this model is that it clearly supports the immediate recognition, in other words, incidental processing of BM stimuli through feedforward processing. So, observing only the form and motion sensitive areas in the OTC during the bottom-up perception of BM under attentional load suggests the need to extend the models like Giese and Poggio (2003)'s or to develop new models. In addition to providing grounds for studying the bottom-up processing of BM, the paradigm used in the present study allows researchers to investigate how attention or attentional load could affect the regions that are involved in bottom-up processing. This top-down effect of attention on the same brain areas highlights the possibility of feedback projections. Thus, our use of the attentional load paradigm in this regard emphasizes the need for more comprehensive models that integrate these two interactive processes and reflect their effect on the overall BM perception. Future studies may look further into building and testing such integrative models.

5. Conclusion

In this study we examined the bottom-up perception of BM under attentional load. We have found that even though the selective attention was directed at an attentionally demanding main task at the fovea, the peripheral task-irrelevant intact and scrambled BM stimuli were processed incidentally. However, the neural correlates of this processing yielded activity that is not specific to BM itself but rather towards the dynamic nature of the stimuli in motion sensitive regions in the OTC. Moreover, the bottom-up processing regions observed in this study were also modulated by attentional load. Thus, our findings provide new grounds for future studies to use the attentional load paradigm to study the stimulus-driven processing models of BM in depth to tackle the interplay between top-down and bottom-up perception of BM.

6. Consent to participate

Prior to the experiment, written informed consent and MRI prescreening form of each participant was collected. After the experiment, participants were compensated for their time.

7. Ethics approval

The study was approved by the Human Research Ethics Committee of Bilkent University in line with the principles of the Declaration of Helsinki.

Funding

H.N. was supported by a graduate student fellowship from a TUBITAK 3501 grant (No: 119K654) awarded to B.A.U.

CRediT authorship contribution statement

Hilal Nizamoglu: Conceptualization, Methodology, Software, Formal analysis, Writing – original draft, Visualization. **Burcu A. Urgen:** Conceptualization, Methodology, Supervision, Funding acquisition.

Declaration of Competing Interest

The authors declare that they have no known competing financial interests or personal relationships that could have appeared to influence the work reported in this paper.

Data availability

The data is available upon reasonable request from the corresponding author.

Acknowledgements

H.N. was supported by a graduate student fellowship from a TUBITAK 3501 grant (No: 119K654) awarded to B.A.U. Moreover, authors would like to thank Damla Çifçi and Şebnem Türe for their help with data collection, and Murat Batu Tunca and Cem Karakuzu for their help with the design of the stimuli.

Appendix A. Supplementary material

Supplementary figures and tables to this article can be found online at https://doi.org/10.1016/j.visres.2023.108328.

References

Abraham, A., Pedregosa, F., Eickenberg, M., Gervais, P., Mueller, A., Kossaifi, J., … Varoquaux, G. (2014). Machine learning for neuroimaging with scikit-learn. *Frontiers in Neuroinformatics, 8*. https://doi.org/10.3389/fninf.2014.00014

Arsalidou, M., Pascual-Leone, J., Johnson, J., Morris, D., & Taylor, M. J. (2013). A balancing act of the brain: Activations and deactivations driven by cognitive load. *Brain and Behavior, 3*(3), 273–285.

Avants, B. B., Epstein, C. L., Grossman, M., & Gee, J. C. (2008). Symmetric diffeomorphic image registration with cross-correlation: Evaluating automated labeling of elderly and neurodegenerative brain. *Medical Image Analysis, 12*(1), 26–41. https://doi.org/10.1016/j.media.2007.06.004

Barré, A. (2013). Motion kinematic and kinetic analyzer (MOKKA). Retrieved from https://biomechanical-toolkit.github.io/mokka/index.html.

Beauchamp, M. S., Lee, K. E., Haxby, J. V., & Martin, A. (2003). FMRI responses to video and point-light displays of moving humans and manipulable objects. *Journal of Cognitive Neuroscience, 15*(7), 991–1001.

Behzadi, Y., Restom, K., Liau, J., & Liu, T. T. (2007). A component based noise correction method (CompCor) for BOLD and perfusion based fMRI. *NeuroImage, 37*(1), 90–101. https://doi.org/10.1016/j.neuroimage.2007.04.042

Bertenthal, B. I., Proffitt, D. R., & Kramer, S. J. (1987). Perception of biomechanical motions by infants: Implementation of various processing constraints. *Journal of Experimental Psychology: Human Perception and Performance, 13*(4), 577.

Blake, R., & Shiffrar, M. (2007). Perception of human motion. *Annual Review of Psychology, 58*, 47–73.

Brainard, D. H. (1997). The psychophysics toolbox. *Spatial Vision, 10*(4), 433–436. https://doi.org/10.1163/156856897X00357

Bruckmaier, M., Tachtsidis, I., Phan, P., & Lavie, N. (2020). Attention and capacity limits in perception: A cellular metabolism account. *Journal of Neuroscience, 40*(35), 6801–6811. https://doi.org/10.1523/JNEUROSCI.2368-19.2020

Buccino, G., Binkofski, F., Fink, G. R., Fadiga, L., Fogassi, L., Gallese, V., … Freund, H.-J. (2001). Action observation activates premotor and parietal areas in a somatotopic manner: An fMRI study. *European Journal of Neuroscience, 13*(2), 400–404. https://doi.org/10.1111/j.1460-9568.2001.01385.x

Chong, T.-T.-J., Williams, M. A., Cunnington, R., & Mattingley, J. B. (2008). Selective attention modulates inferior frontal gyrus activity during action observation. *NeuroImage, 40*(1), 298–307. https://doi.org/10.1016/j.neuroimage.2007.11.030

Corbetta, M., Kincade, J. M., Ollinger, J. M., McAvoy, M. P., & Shulman, G. L. (2000). Voluntary orienting is dissociated from target detection in human posterior parietal cortex. *Nature Neuroscience, 3*(3), 292–297.

Corbetta, M., Patel, G., & Shulman, G. L. (2008). The reorienting system of the human brain: From environment to theory of mind. *Neuron, 58*(3), 306–324. https://doi.org/10.1016/j.neuron.2008.04.017

Cox, R. W., & Hyde, J. S. (1997). Software tools for analysis and visualization of fMRI data. *NMR in Biomedicine, 10*(4–5), 171–178. https://doi.org/10.1002/(SICI)1099-1492(199706/08)10:4/5<171::AID-NBM453>3.0.CO;2-L

Dale, A. M., Fischl, B., & Sereno, M. I. (1999). Cortical surface-based analysis: I. Segmentation and surface reconstruction. *NeuroImage, 9*(2), 179–194. https://doi.org/10.1006/nimg.1998.0395

Danielmeier, C., Eichele, T., Forstmann, B. U., Tittgemeyer, M., & Ullsperger, M. (2011). Posterior medial frontal cortex activity predicts post-error adaptations in task-related visual and motor areas. *Journal of Neuroscience, 31*(5), 1780–1789.

Davis, T., LaRocque, K. F., Mumford, J. A., Norman, K. A., Wagner, A. D., & Poldrack, R. A. (2014). What do differences between multi-voxel and univariate analysis mean? How subject-, voxel-, and trial-level variance impact fMRI analysis. *NeuroImage, 97*, 271–283. https://doi.org/10.1016/j.neuroimage.2014.04.037

de C. Hamilton, A. F., & Grafton, S. T. (2007). Action outcomes are represented in human inferior frontoparietal cortex. *Cerebral Cortex, 18*(5), 1160–1168. doi: 10.1093/cercor/bhm150.

Desseilles, M., Balteau, E., Sterpenich, V., Dang-Vu, T. T., Darsaud, A., Vandewalle, G., … Schwartz, S. (2009). Abnormal neural filtering of irrelevant visual information in depression. *Journal of Neuroscience, 29*(5), 1395–1403. https://doi.org/10.1523/JNEUROSCI.3341-08.2009

Downing, P. E., Jiang, Y., Shuman, M., & Kanwisher, N. (2001). A cortical area selective for visual processing of the human body. *Science, 293*(5539), 2470–2473.

Esteban, O., Blair, R., Markiewicz, C. J., Berleant, S. L., Moodie, C., Ma, F., … Gorgolewski, K. J. (2018). fMRIPrep. *Software*. https://doi.org/10.5281/zenodo.852659

Esteban, O., Markiewicz, C., Blair, R. W., Moodie, C., Isik, A. I., Erramuzpe Aliaga, A., … Gorgolewski, K. J. (2018). fMRIPrep: A robust preprocessing pipeline for functional MRI. *Nature Methods*. https://doi.org/10.1038/s41592-018-0235-4

Felleman, D. J., & Van Essen, D. C. (1991). Distributed hierarchical processing in the primate cerebral cortex. *Cerebral Cortex, 1*(1), 1–47.

Fonov, V. S., Evans, A. C., McKinstry, R. C., Almli, C. R., & Collins, D. L. (2009). Unbiased nonlinear average age-appropriate brain templates from birth to adulthood. *NeuroImage, 47*(Supplement 1), S102. https://doi.org/10.1016/S1053-8119(09)70884-5

Forster, S., & Lavie, N. (2008). Attentional capture by entirely irrelevant distractors. *Visual Cognition, 16*(2–3), 200–214.

Fox, R., & McDaniel, C. (1982). The perception of biological motion by human infants. *Science, 218*(4571), 486–487.

Giese, M. A., & Poggio, T. (2003). Neural mechanisms for the recognition of biological movements. *Nature Reviews Neuroscience, 4*(3), 179–192.

Gorgolewski, K., Burns, C. D., Madison, C., Clark, D., Halchenko, Y. O., Waskom, M. L., & Ghosh, S. (2011). Nipype: A flexible, lightweight and extensible neuroimaging data processing framework in Python. *Frontiers in Neuroinformatics, 5*, 13. https://doi.org/10.3389/fninf.2011.00013

Gorgolewski, K. J., Esteban, O., Markiewicz, C. J., Ziegler, E., Ellis, D. G., Notter, M. P., … Ghosh, S. (2018). Nipype. *Software*. https://doi.org/10.5281/zenodo.596855

Greve, D. N., & Fischl, B. (2009). Accurate and robust brain image alignment using boundary-based registration. *NeuroImage, 48*(1), 63–72. https://doi.org/10.1016/j.neuroimage.2009.06.060

Grezes, J., Fonlupt, P., Bertenthal, B., Delon-Martin, C., Segebarth, C., & Decety, J. (2001). Does perception of biological motion rely on specific brain regions? *NeuroImage, 13*(5), 775–785.

Grossman, E. D., & Blake, R. (2002). Brain areas active during visual perception of biological motion. *Neuron, 35*(6), 1167–1175.

Grossman, E. D., Blake, R., & Kim, C.-Y. (2004). Learning to see biological motion: Brain activity parallels behavior. *Journal of Cognitive Neuroscience, 16*(9), 1669–1679.

Halovic, S., & Kroos, C. (2018). Walking my way? Walker gender and display format confounds the perception of specific emotions. *Human Movement Science, 57*, 461–477.

Hebart, M. N., Görgen, K., & Haynes, J.-D. (2015). The Decoding Toolbox (TDT): A versatile software package for multivariate analyses of functional imaging data. *Frontiers in Neuroinformatics, 8*. https://doi.org/10.3389/fninf.2014.00088

Herrington, J., Nymberg, C., Faja, S., Price, E., & Schultz, R. (2012). The responsiveness of biological motion processing areas to selective attention towards goals. *NeuroImage, 63*(1), 581–590.

Jastorff, J., Begliomini, C., Fabbri-Destro, M., Rizzolatti, G., & Orban, G. A. (2010). Coding observed motor acts: Different organizational principles in the parietal and premotor cortex of humans. *Journal of Neurophysiology, 104*(1), 128–140. https://doi.org/10.1152/jn.00254.2010

Jastorff, J., & Orban, G. A. (2009). Human functional magnetic resonance imaging reveals separation and integration of shape and motion cues in biological motion processing. *Journal of Neuroscience, 29*(22), 7315–7329.

Jastorff, J., Popivanov, I. D., Vogels, R., Vanduffel, W., & Orban, G. A. (2012). Integration of shape and motion cues in biological motion processing in the monkey STS. *NeuroImage, 60*(2), 911–921.

Jenkins, A. C. (2019). Rethinking cognitive load: A default-mode network perspective. *Trends in Cognitive Sciences, 23*(7), 531–533. https://doi.org/10.1016/j.tics.2019.04.008

Jenkinson, M., Bannister, P., Brady, M., & Smith, S. (2002). Improved optimization for the robust and accurate linear registration and motion correction of brain images. *NeuroImage, 17*(2), 825–841. https://doi.org/10.1006/nimg.2002.1132

Johansson, G. (1973). Visual perception of biological motion and a model for its analysis. *Perception & Psychophysics, 14*(2), 201–211.

Klein, A., Ghosh, S. S., Bao, F. S., Giard, J., Häme, Y., Stavsky, E., … Keshavan, A. (2017). Mindboggling morphometry of human brains. *PLOS Computational Biology, 13*(2), e1005350.

Kleiner, M., Brainard, D., Pelli, D., Ingling, A., Murray, R., & Broussard, C. (2007). What's new in psychtoolbox-3. *Perception, 36*(14), 1–16.

Lanczos, C. (1964). Evaluation of noisy data. *Journal of the Society for Industrial and Applied Mathematics Series B Numerical Analysis, 1*(1), 76–85. https://doi.org/10.1137/0701007

Lavie, N. (1995). Perceptual load as a necessary condition for selective attention. *Journal of Experimental Psychology: Human Perception and Performance, 21*(3), 451–468. https://doi.org/10.1037/0096-1523.21.3.451

Lavie, N. (2005). Distracted and confused?: Selective attention under load. *Trends in Cognitive Sciences, 9*(2), 75–82. https://doi.org/10.1016/j.tics.2004.12.004

Lesage, E., & Stein, E. A. (2016). Networks associated with reward. In N. Y. New York (Ed.), *Neuroscience in the 21st century* (pp. 1–27). York: Springer, New.

Lleras, A., Chu, H., & Buetti, S. (2017). Can we "apply" the findings of Forster and Lavie (2008)? On the generalizability of attentional capture effects under varying levels of perceptual load. *Journal of Experimental Psychology: Applied, 23*(2), 158.

Menon, V. (2011). Large-scale brain networks and psychopathology: A unifying triple network model. *Trends in Cognitive Sciences, 15*(10), 483–506. https://doi.org/10.1016/j.tics.2011.08.003

Oram, M. W., & Perrett, D. I. (1996). Integration of form and motion in the anterior superior temporal polysensory area (STPa) of the macaque monkey. *Journal of Neurophysiology, 76*(1), 109–129.

Pavlova, M., Krägeloh-Mann, I., Sokolov, A., & Birbaumer, N. (2001). Recognition of point-light biological motion displays by young children. *Perception, 30*(8), 925–933.

Peelen, M. V., Wiggett, A. J., & Downing, P. E. (2006). Patterns of fMRI activity dissociate overlapping functional brain areas that respond to biological motion. *Neuron, 49*(6), 815–822.

Pelli, D. G. (1997). The VideoToolbox software for visual psychophysics: Transforming numbers into movies. *Spatial Vision, 10*(4), 437–442. https://doi.org/10.1163/156856897X00366

Penny, W. D., Friston, K. J., Ashburner, J. T., Kiebel, S. J., & Nichols, T. E. (2011). Statistical parametric mapping: The analysis of functional brain images. Elsevier.

Peuskens, H., Vanrie, J., Verfaillie, K., & Orban, G. A. (2005). Specificity of regions processing biological motion. *European Journal of Neuroscience, 21*(10), 2864–2875.

Pitcher, D., & Ungerleider, L. G. (2021). Evidence for a third visual pathway specialized for social perception. *Trends in Cognitive Sciences, 25*(2), 100–110. https://doi.org/10.1016/j.tics.2020.11.006

Pollick, F. E., Kay, J. W., Heim, K., & Stringer, R. (2005). Gender recognition from point-light walkers. *Journal of Experimental Psychology: Human Perception and Performance, 31*(6), 1247.

Power, J. D., Mitra, A., Laumann, T. O., Snyder, A. Z., Schlaggar, B. L., & Petersen, S. E. (2014). Methods to detect, characterize, and remove motion artifact in resting state fMRI. *NeuroImage, 84*(Supplement C), 320–341. https://doi.org/10.1016/j.neuroimage.2013.08.048

Pyles, J. A., & Grossman, E. D. (2013). Neural Mechanisms for Biological Motion and Animacy. In K. L. Johnson, and M. Shiffrar (Eds.), *People watching: Social, perceptual, and neurophysiological studies of body perception* (pp. 304–317). Oxford University Press.

Raichle, M. E. (2015). The Brain's Default Mode Network. *Annual Review of Neuroscience, 38*(1), 433–447. https://doi.org/10.1146/annurev-neuro-071013-014030

Rauss, K., Pourtois, G., Vuilleumier, P., & Schwartz, S. (2012). Effects of attentional load on early visual processing depend on stimulus timing. *Human Brain Mapping, 33*(1), 63–74. https://doi.org/10.1002/hbm.21193

Rees, G., Frith, C. D., & Lavie, N. (1997). Modulating irrelevant motion perception by varying attentional load in an unrelated task. *Science, 278*(5343), 1616–1619. https://doi.org/10.1126/science.278.5343.1616

Reuter, M., Rosas, H. D., & Fischl, B. (2010). Highly accurate inverse consistent registration: A robust approach. *NeuroImage, 53*(4), 1181–1196. https://doi.org/10.1016/j.neuroimage.2010.07.020

Rizzolatti, G., & Craighero, L. (2004). The mirror-neuron system. *Annual Review of Neuroscience, 27*(1), 169–192. https://doi.org/10.1146/annurev.neuro.27.070203.144230

Rizzolatti, G., Fadiga, L., Gallese, V., & Fogassi, L. (1996). Premotor cortex and the recognition of motor actions. *Cognitive Brain Research, 3*, 131–141. https://doi.org/10.1016/0926-6410(95)00038-0

Rutherford, M. D., & Kuhlmeier, V. A. (Eds.). (2013). *Social perception: Detection and interpretation of animacy, agency, and intention.* MIT Press.

Satterthwaite, T. D., Elliott, M. A., Gerraty, R. T., Ruparel, K., Loughead, J., Calkins, M. E., … Wolf, D. H. (2013). An improved framework for confound regression and filtering for control of motion artifact in the preprocessing of resting-state functional connectivity data. *NeuroImage, 64*(1), 240–256. https://doi.org/10.1016/j.neuroimage.2012.08.052

Saygin, A. P., & Sereno, M. I. (2008). Retinotopy and attention in human occipital, temporal, parietal, and frontal cortex. *Cerebral Cortex, 18*(9), 2158–2168. https://doi.org/10.1093/cercor/bhm242

Saygin, A. P., Wilson, S. M., Hagler, D. J., Bates, E., & Sereno, M. I. (2004). Point-light biological motion perception activates human premotor cortex. *Journal of Neuroscience, 24*(27), 6181–6188.

Saygin, A. P. (2013). Sensory and motor brain areas supporting biological motion perception: Neuropsychological and neuroimaging studies. In K. L. Johnson, and M. Shiffrar (Eds.), *People watching: Social, perceptual, and neurophysiological studies of body perception* (pp. 369–387). Oxford University Press.

Schwartz, S., Vuilleumier, P., Hutton, C., Maravita, A., Dolan, R. J., & Driver, J. (2004). Attentional load and sensory competition in human vision: Modulation of fMRI responses by load at fixation during task-irrelevant stimulation in the peripheral visual field. *Cerebral Cortex, 15*(6), 770–786. https://doi.org/10.1093/cercor/bhh178

Shiffrar, M. (1994). When what meets where. *Current Directions in Psychological Science, 3*(3), 96–101.

Sifre, R., Olson, L., Gillespie, S., Klin, A., Jones, W., & Shultz, S. (2018). A longitudinal investigation of preferential attention to biological motion in 2-to 24-month-old infants. *Scientific Reports, 8*(1), 2527.

Simion, F., Regolin, L., & Bulf, H. (2008). A predisposition for biological motion in the newborn baby. *Proceedings of the National Academy of Sciences, 105*(2), 809–813.

Thompson, J., & Parasuraman, R. (2012). Attention, biological motion, and action recognition. *NeuroImage, 59*(1), 4–13.

Thoresen, J. C., Vuong, Q. C., & Atkinson, A. P. (2012). First impressions: Gait cues drive reliable trait judgements. *Cognition, 124*(3), 261–271.

Thornton, I. M., Rensink, R. A., & Shiffrar, M. (2002). Active versus passive processing of biological motion. *Perception, 31*(7), 837–853. https://doi.org/10.1068/p3072

Thornton, I. M., & Vuong, Q. C. (2004). Incidental processing of biological motion. *Current Biology, 14*(12), 1084–1089. https://doi.org/10.1016/j.cub.2004.06.025

Thornton, I. M. (2013). Top-down versus Bottom-up Processing of Biological Motion. In K. L. Johnson, and M. Shiffrar (Eds.), *People watching: Social, perceptual, and neurophysiological studies of body perception* (pp. 25–43). Oxford University Press.

Tustison, N. J., Avants, B. B., Cook, P. A., Zheng, Y., Egan, A., Yushkevich, P. A., & Gee, J. C. (2010). N4ITK: improved N3 bias correction. *IEEE Transactions on Medical Imaging, 29*(6), 1310–1320. https://doi.org/10.1109/TMI.2010.2046908

Urgen, B. A., & Orban, G. A. (2021). The unique role of parietal cortex in action observation: Functional organization for communicative and manipulative actions. *NeuroImage, 237*, Article 118220. https://doi.org/10.1016/j.neuroimage.2021.118220

Vaina, L. M., Solomon, J., Chowdhury, S., Sinha, P., & Belliveau, J. W. (2001). Functional neuroanatomy of biological motion perception in humans. *Proceedings of the National Academy of Sciences, 98*(20), 11656–11661.

Vallortigara, G., Regolin, L., & Marconato, F. (2005). Visually inexperienced chicks exhibit spontaneous preference for biological motion patterns. *PLoS Biology, 3*(7), e208.

van Boxtel, J. J. A., & Lu, H. (10 2013). A biological motion toolbox for reading, displaying, and manipulating motion capture data in research settings. *Journal of Vision, 13*(12), 7–7. doi: 10.1167/13.12.7.

Vangeneugden, J., De Mazière, P. A., Van Hulle, M. M., Jaeggli, T., Van Gool, L., & Vogels, R. (2011). Distinct mechanisms for coding of visual actions in macaque temporal cortex. *Journal of Neuroscience, 31*(2), 385–401. https://doi.org/10.1523/JNEUROSCI.2703-10.2011

Vangeneugden, J., Peelen, M. V., Tadin, D., & Battelli, L. (2014). Distinct neural mechanisms for body form and body motion discriminations. *Journal of Neuroscience, 34*(2), 574–585.

Vangeneugden, J., Pollick, F., & Vogels, R. (2008). Functional differentiation of macaque visual temporal cortical neurons using a parametric action space. *Cerebral Cortex, 19*(3), 593–611. https://doi.org/10.1093/cercor/bhn109

Wheaton, K. J., Thompson, J. C., Syngeniotis, A., Abbott, D. F., & Puce, A. (2004). Viewing the motion of human body parts activates different regions of premotor, temporal, and parietal cortex. *NeuroImage, 22*(1), 277–288. https://doi.org/10.1016/j.neuroimage.2003.12.043

Yovel, G., & O'Toole, A. J. (2016). Recognizing people in motion. *Trends in Cognitive Sciences, 20*(5), 383–395.

Zhang, Y., Brady, M., & Smith, S. (2001). Segmentation of brain MR images through a hidden Markov random field model and the expectation-maximization algorithm. *IEEE Transactions on Medical Imaging, 20*(1), 45–57. https://doi.org/10.1109/42.906424